Journal of Electronics and Electrical Engineering
https://ojs.wiserpub.com/index.php/JEEE

Research Article

Design, Fabrication and Experimental Validation of a Piezoelectric Energy Harvester for Smart Vehicles

Zaryab Basharat[1,2*], Muhammad Zaid Buzal [2], Muhammad Haris Malik[2,3], Wania Saleem[4]

[1] MOE Key Laboratory of Thermo-Fluid Science and Engineering, Xi'an Jiaotong University, Xi'an, China
[2] Department of Mechanical Engineering, University of Engineering and Technology Lahore (Narowal Campus), Narowal, Pakistan
[3] Department of Fluid Machinery and Engineering, Xi'an Jiaotong University, Xi'an, China
[4] Department of Chemistry, University of Engineering and Technology Lahore, Lahore, Pakistan
* Correspondence: 2020me521@student.uet.edu.pk

Received: 14 January 2026; **Revised:** 8 February 2026; **Accepted:** 26 February 2026; **Published:** 10 March 2026

Abstract: Piezoelectricity has become the focus of researchers because of the ability of piezoelectric materials to convert applied mechanical stress into electricity. There has been a great interest in harvesting energy from vibrations generated by car engine in running condition. Suitable energy harvester can be used to convert these vibrations into electricity. In this research, we have designed a piezoelectric cantilever beam type configuration for energy harvesting from engine's vibrations. Number of calculations are made and the disk shape of PZT-5A having 36 mm diameter is selected. Every disc of PZT-5A has a diameter of 36 mm, meaning it has an active area of nearly 9.62 cm^2, making up an aggregate area of 67.3 cm^2 for seven discs, a damping factor of 0.03 was assumed. The harvested energy is then temporarily stored in the capacitor bank. The battery control unit is designed using Raspberry Pi microcontroller, which controls the battery supply. When battery is charged to certain limit then, it will stop charging the battery and supply is directly applied to load, and when battery is below certain limit, then it will charge the battery first. Both analytical and simulation-based results are obtained and there has been a close match. A cantilever beam with piezoelectric attached is designed and fabricated using the simulation and analytical results. The system is then mounted on engine' head and experiments were performed for 500, 750, 1,000, 1,250, and 1,500 rpms and output voltages were noted as 14.51, 9.47, 7.14, 6.69 and 5.17 volts respectively. It was concluded that there has been a close match with analytical results. Experimental validation with the engine mounted in the running vehicle has proved the concept's validity with regards to the use of waste engine vibrations for the generation of sustainable energy.

Keywords: piezoelectric, vehicles, PZT, voltage, cantilever beam, Raspberry Pi

1. Introduction

Piezoelectric Energy Harvesting (PEH) involves the utilization of materials that can generate an electrical charge when subjected to mechanical stress. By integrating piezoelectric elements into various components of the vehicle, such as the suspension system, tires, body panels, and seats, the mechanical vibrations generated during the vehicle's operation can be harnessed and transformed into usable electrical energy. It is the property of piezoelectric materials that when subjected to stress or deformation, produce electricity. Most common such materials used in energy harvesters include lead zirconate

DOI: https://doi.org/10.37256/jeee.5120269605

titanate (PZT), polyvinylidene fluoride (PVDF), and others. The benefits of PEH in smart vehicles are manifold. It offers a renewable and sustainable energy source, reducing dependence on traditional energy sources and minimizing the carbon footprint.

The piezoelectric energy harvester of cantilever beam type configuration is shown in Figure 1. It is shown that tip mass is attached to the end of cantilever beam which aids in the mechanical vibrations. The piece of piezoelectric material is attached at the top of beam with electrical wires. When the beam vibrates, material absorbs the vibrations and convert them into electrical energy, which is stored in the energy storage system. The piezoelectric components and their attachment and mounting features are shown in the Figure 2.

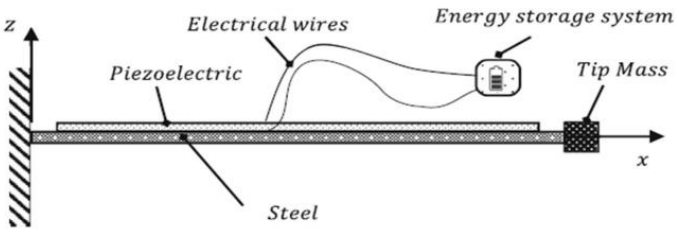

Figure 1. Clamped-free piezo-harvester [1]

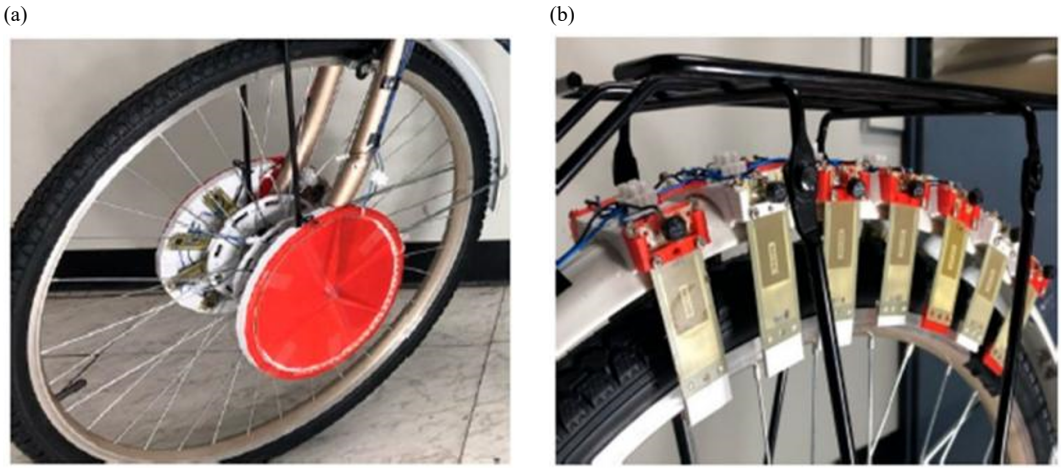

Figure 2. Installation of piezoelectric modules on a bicycle [1]

In recent years, many publications and prototypes have been presented related to the field of energy harvesting and thus this field has become important. There are also different excellent variations of mechanisms and methods that have been published on this topic [2]. PEH has become a focused topic in the literature and gained great concern from scholars because of its advantages of simple structure, large power density, and good scalability [3].

The increased demand and popularity of smart automobiles have pushed the demand for efficient and clean power solutions. Conventional power sources, such as internal combustion engines and batteries, are constrained in terms of efficiency in energy usage, environmental expense, and dependence on external charging facilities. In a bid to overcome such limitations, scientists and engineers have been looking for alternative methods of harnessing energy from the environment surrounding the vehicle. Energy harvesting is the collection and utilization of ambient or environment-based energy sources in charging electronic systems or devices. Piezoelectricity is the generation of electricity from mechanical stress/deformation through the utilization of special materials with piezoelectric properties. Figure 3 demonstrates the

mounting of cantilever harvester on a vehicle under the application of VFC strategy to load resistance. It shows the working of VFC on small city car and its numerical simulations.

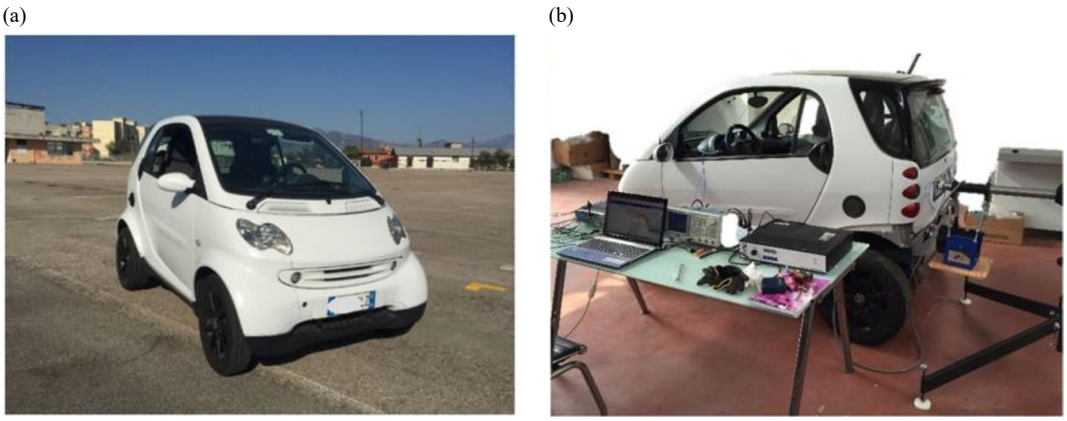

Figure 3. Smart vehicle system [4]

In the rapidly evolving climate of electric and intelligent transport, there is a fundamental need to develop sustainable and reliable sources of power to power the various operating mechanisms and systems in these vehicles. One such probable remedy is incorporating PEH technology, which has the potential to convert mechanical vibrations and stress encountered by a moving vehicle into electricity.

The aim of the research in this work is to design and position the piezoelectric elements in key locations in the vehicle to harvest maximum energy. The primary objective of PEH is to enhance the energy efficiency of smart vehicles. PEH systems can supplement or even replace conventional power sources by capturing and converting mechanical vibrations into electrical energy, hence reducing the overall energy consumption of the vehicle. Another important objective is to facilitate sustainable power generation in smart vehicles.

The research will be focused on enhancing the efficiency of PEH using mechanical vibrations and strain produced during vehicle operation. Energy storage and management systems for storing and distributing harnessed energy efficiently to power smart vehicle components will also form a part of this research. This research will explore cost-effective manufacturing methods and materials to make the technology economically viable for the automotive industry. The environmental impact of the technology will be assessed and minimized, considering factors such as materials used and disposal at the end of life. Since, we know that vibrations are everywhere, and vibration-based energy harvesters will come to our real life.

The study's specific objectives are to design and construct a multi-disc piezoelectric cantilever energy harvester for engine mounting use, experimentally study the voltage production for various engine speeds ranging from 500 to 1500 RPM, numerical analysis for dynamic and electric responses by finite element model, compare the proposed design and the existing reference design to assess the improvement in performance.

The limitations of this research include the need for developing piezoelectric materials with higher coupling coefficients to significantly enhance energy conversion efficiency, the requirement for flexible and durable materials capable of withstanding extreme vibrations and shocks, and the necessity of efficient electronic circuits for rectification and energy storage due to the low output voltage generated from vibrations. Currently available engine-mounted piezoelectric harvesters have limitations in terms of low energy density, low performance during non-resonant conditions, and low voltage levels because of the patch arrangement. In addition, the majority of published studies have been focused on lab-scale experiments rather than those suitable for vehicle-scale implementation. This problem is addressed through the use of a multi-disc approach for the design of the cantilever arrangement based on the engine-induced broadband vibrations of the vehicle.

1.1 *Components of an energy harvester*

The main components of an energy harvester consisting piezoelectric typically include piezoelectric materials, transducers, electrodes, mechanical coupling mechanism, electrical interface, mounting and attachment features.

Piezoelectric material is the core component of the energy harvester. Piezoelectric materials have the property of generating an electric charge when subjected to mechanical stress or deformation. The piezoelectric materials which are used commonly for energy harvesting include PZT, PVDF, and others. The most common configurations of PEH devices are unimorph (one layer of piezoelectric material bonded to a non-piezoelectric layer) or a bimorph (two layers of piezoelectric material bonded to a non-piezoelectric layer) with a cantilever design. These materials have emerged into a dominant role of sonic and the low ultrasonic range of piezoelectric transducers [5].

The piezoelectric typically occurs in transducer form. Upon input of mechanical energy to the transducer (e.g., vibrations or pressure fluctuations), it becomes deformed, resulting in an electrical charge as a consequence of the mechanical stress. To this end, electrodes are attached to the faces of the piezoelectric material in order to collect the electric charge generated when deformed. These will conduct the produced electrical energy to an external circuit. The energy harvester may include a mechanical coupling mechanism for effectively collecting the mechanical energy from the environment. The mechanism may provide for the transfer and amplification of the mechanical vibrations or deformations to the piezoelectric transducer. Piezoelectric material harvests energy that needs to be conditioned and processed for effective application. The processing includes an electrical interface that normally incorporates a rectifier, regulation of the voltage, and storage elements like capacitors or batteries.

The kinetic regulation of the harvester can be achieved by the passive tuning of the stiffness and damping of the spring-cantilever system to yield near-resonant operation over a wider RPM range. This kinetic regulation ensures stable and regulated vibration amplitude for fluctuating excitation. Energy conversion efficiency can be improved under fluctuating excitation due to the maintenance of effective electromechanical coupling, as noted in recent kinetic regulation strategies represented in the literature on vibration energy harvesting.

According to the application, the harvester of energy can attach or mount the device on the mechanical energy source with adhesive surfaces, clamps, or brackets. Figure 2 represents some of the mounting features of a PEH system. All the components are integrated into single components which is then mounted on the selected part of the vehicle.

1.2 *Design considerations*

In designing a successful Piezoelectric Energy Harvesting system for intelligent vehicles, some critical considerations must be made. These include the careful selection of piezoelectric material, considering efficiency, toughness, and cost; the careful integration of the harvesting mechanism with vehicle parts such as suspension, tires, and body panels; the application of efficient mechanisms related to power storage and management to allow for consistent energy supply; and enabling cost minimization and scaling up for mass production to enable broader usage on models of smart vehicles.

1.3 *Design procedure*

The system design of a Piezoelectric Energy Harvesting (PEH) system involves the proper design and optimization of piezoelectric elements from the sources of vehicle vibrations, using analytical modeling, simulations, and Finite Element Analysis (FEA) for enhancing the efficiency of energy conversion. Different types include unimorphs, bimorphs, and cantilever types for better performance [6]. Prototyping and integration need special mounts and electrical interfaces to maintain the correct alignment of the different components in a vehicle. An efficient system of power storage and management is also developed, with supplementation by rectifiers, voltage regulators, and storage elements. The final process is performance testing under real-world conditions in order to find the efficiency, output power, and reliability, optimized for peak system performance [7].

1.4 *Expected results*

The main novelties of this study include the incorporation of a multi-disc PZT configuration with a spring-assisted cantilever for increased strain concentration, easier integration in engine mounts, and experimental verification under realistic engine operating conditions. Structural simplicity, scalability, and ease of fabrication were emphasized in the design and fabrication process as key factors for practical manufacture in a vehicular context. The expected outcomes of this research are improved energy efficiency in smart vehicles by using a PEH system that can generate adequate electrical power to devices such as sensors, communication systems, lighting, and auxiliary devices. It is expected that the system could be easily connected within different parts of the vehicle, minimizing added weight while keeping aesthetic appearances and harvesting maximum vibration energy. It is also expected to show reliability and resistance to harsh operating conditions. Overall, the PEH system will improve sustainability, power management, cost-effectiveness, and intelligent vehicle performance and independence.

It is concluded that Piezoelectric Energy Harvesting (PEH) systems design and deployment in smart cars have immense potential to enhance energy efficiency, make sustainability feasible, and reduce the reliance on external power supplies. With the successful integration of PEH systems in different car components, mechanical vibrations can be harvested and transduced into usable electrical energy, greening the transportation system and making it more autonomous.

2. Literature review

Bailey and Hubbard Jr. [8] offered one of the first studies on active vibration control of cantilever beams using a distributed piezoelectric-polymer actuator. They employed polyvinylidene fluoride (PVDF) as a distributed-parameter actuator, supplemented by distributed-parameter control theory. They employed a control algorithm formulated based on Lyapunov's second method for all beam modes' control of vibrations, in terms of known tip angular velocity. Their experimental observation was a baseline loss factor of 0.003 in large-amplitude vibrations (±2 cm) decreasing to 0.001 for small vibrations (±0.5 mm). Using a constant-gain controller under a 200 V rms voltage limit, the damping was more than doubled. Moreover, a constant-amplitude controller achieved similar damping for large vibrations and significantly enhanced damping at small amplitudes, with the modal loss factor increasing to at least 0.040. This study marked an important step forward in the application of piezoelectric polymers to distributed active vibration control in flexible structures [9].

Because of the associated benefits, there have been a number of experiments carried out using the flexible organic-type PVDF to produce the PVDF film. This includes the experiment carried out by Maurya et al. [10]. From the observation made on the experiment, the higher the vehicle speed and the greater the thickness of the piezoelectric material, the greater the possible voltage generated. Though the 2 mm material thickness generates a slight reduction in the magnitude of the voltage generated, the observation clearly indicates that the artificial harvester for the piezoelectric material is capable of turning on 78 Light-Emitting Diodes (LEDs) at a power of 580 μW. In a study, Ikbal et al. [11] utilized a silicone-based adhesive to mount three PVDF films with a thickness of 200 μm into the interior layer of the tire achieving a maximum voltage of around 16 V.

Tang and Wang [12] gave a comparison study between active-passive hybrid piezoelectric networks for vibration control, based on the evaluation of passive damping and active controllability across different configurations of piezoelectric spines. The analysis was made in a non-dimensional framework, emphasizing the central role of the total electromechanical coupling factor. Their results show that various configurations yielded similar open-loop performance when operated under the same conditions of electromechanical switching. It is indicated herein that the increase in the electromechanical coupling factor has improved the passive damping effectiveness and also, under specific configurations, increased the power of active control and the overall system efficiency. The authors further proposed and experimentally demonstrated a method to increase the coupling factor through a negative capacitance circuit, an opportunity for improved hybrid vibration control system performance.

Vidoli and Dell'Isola [13] introduced a novel method of controlling plate vibration with a continuously distributed control system of coupled piezoelectric (PZT) actuators.

The distributed actuators are equally spread in the plate and serve both as capacitive devices in an electric network and as mechanical coupling providers simultaneously. The authors formulated a self-resonance condition that ensures successful electro-mechanical energy transfer from the plate to the electric network. Their work solved vibration control of clamped and simply supported plates, and they determined optimal network impedance for maximum performance. The results demonstrated that the proposed system significantly enhances the performance of piezoelectric actuation in vibration suppression applications [14]. Uchino [15] provides an overview of piezoelectric transducers and actuators. He chronicles the history of the piezoelectric effect from its discovery by Pierre and Jacques Curie in 1880. Both the direct piezoelectric effect-where electric charge is produced by mechanical stress-and the converse effect, where an electric field produces mechanical strain, are documented in the study.

Uchino [15] identifies five prevailing performance parameters for piezoelectric materials: strain constant (d), voltage constant (g), electromechanical coupling factor (k), mechanical quality factor (Q), and acoustic impedance (Z). The study focuses on the increasing role of piezoelectric and electro-strictive materials in smart actuator systems such as precision positioners, ultrasonic motors, adaptive dampers, and vibration attenuation in aerospace and military applications. Of the actuator configurations, the multilayer structures possess high force and low voltage with fast response but small displacement, while bimorph actuators have bigger displacement with reduced force and slow response. This foundation work identifies the tradeoffs among force, displacement, and responsiveness in piezoelectric actuator design, which guides their applications in a wide range of engineering fields [16].

Kitagawa et al. [17] described the properties and engineering applications of piezoelectric dampers in smart structural systems for tall buildings. Drawing upon previous work that emphasized the three-dimensional roles which the piezoelectric material can take on-sensors, actuators, and dampers-the research focused on the performance evaluation of piezoelectric material-embedded cantilever beams. The authors explained that piezoelectric dampers work to perform their function using the piezoelectric effect, a process by which mechanical strain is converted into electrical energy. This energy is then dissipated as heat through a shunted circuit comprised of resistors, inductors, and capacitors; thus, the vibrations within the building are damped. Results emphasize the potential of piezoelectric dampers in improving the dynamic properties and safety of high-rise buildings; thus, being effective as an energy-dissipating technology within smart structural systems.

Roundy [18] discusses the performance of the vibration-based energy harvesting systems and performs a comparative analysis of different technologies and designs in the topic. Considering the complexity of the comparison of the various approaches developed for energy harvesting, the research proposes a theoretical framework for estimating optimum power densities for commonly encountered vibration environments. The potential energy outputs for a wide variety of vibration scenarios appear to be in the range from 0.5 to 100 mW/cm^3 for oscillations of 1–10 m/s^2 at frequencies of 50–350 Hz. The key parameters influencing power output will be the electromechanical coupling coefficient of the system, the quality factor of the harvester, the mass density of the generator, and the electrical load matching. The present work provides valuable background for understanding and comparing the energy efficiency of different vibration-based energy harvesting systems and points out the role of system parameters to achieve optimum performance.

Moheimani and Fleming [19] introduce basic concepts of piezoelectricity, this time focusing on the actuation mechanism in beams through collocated piezoelectric transducers. They have introduced an arrangement where two pieces of PZT patches are bonded on opposite surfaces of a beam. If identical but opposite-phase voltages (180° out of phase) are applied, one patch will extend and the other will contract, generating a bending moment in the beam but not longitudinal waves. This pure bending therefore demonstrates the fundamental actuation mechanism of piezoelectric systems. This work gives important insight into the possibilities of controlled electrical inputs to directly induce mechanical deformation, thereby giving a basis for effective design of piezoelectric actuators in vibration control and structural health monitoring.

The work of Moheimani and Fleming [19] investigates the role of piezoelectric materials, particularly PZT ceramics, in vibration control and damping. Piezoelectricity is the quality of electricity generated from pressure-a quality inherent to some materials such as quartz and topaz. Because of its high electro-mechanical coupling factor which enables them to generate large voltage at low displacement, PZT ceramics are used in vibration applications. The work identifies the application of piezoelectric shunt damping, an enormously desired technique to dampen flexible structures, wherein an electrical impedance is connected to a piezoelectric transducer bonded on the structure. This method does not include external sensors and gives huge stabilization. The authors cited Hollkamp, who had designed the first multi-mode shunt

circuit, where the second and third modes of a cantilever beam were successfully damped. In the paper, the emphasis was placed on how piezoelectric shunt damping increases performance and stability in dynamic systems [20].

Sohn et al. [21] investigated the active vibration control of a smart hull structure with Macro-Fiber Composite (MFC) actuators. The active vibration control system was formulated in state-space form based on the equations of motion that were derived using Donnell-Mushtari shell theory. The modal characteristics were also analyzed and compared with finite element and experimental results. A Linear Quadratic Gaussian (LQG) control algorithm was implemented. Experimental verification of vibration control shows the effectiveness of the controller in active reduction of vibrations.

Figure 4 Experimental setup with cantilever aluminum beam mounted with a piezoelectric element 282 mm from the fixed end. A piezoelectric circuit is attached along with a multimeter. One end of the beam is fixed with a rigid frame mounted on the engine foundation, and the free end is suspended near the most vibrating part of the engine, very close to the block head, which can effectively transfer the vibration for efficient energy harvesting from the engine's vibrations.

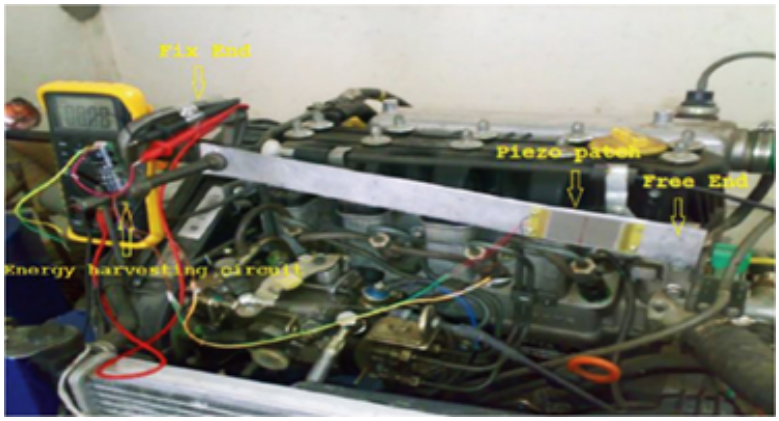

Figure 4. Reference model

Shafer and Garcia investigate the fundamental limits on power and efficiency for cantilevered piezoelectric energy harvesters. While the majority of prior models have targeted the analysis for a particular harvester design and assumed power output to increase linearly with input acceleration, the work considers such a system to be bound by an upper limit imposed by the ultimate strength of the piezoelectric material. The authors derive analytical expressions for the maximum input acceleration and output power and consider an idealized design approach to describe performance for a wide range of system masses and excitation frequencies. The research also discusses general efficiency limits for piezoelectric harvesting devices [7].

Khalatkar and Gupta [22] describe the investigation of piezoelectric materials as ways to harvest energy from low engine vibrations. This would help to power sensors and batteries in smart vehicles. Yingyong et al. [23] examined the effects of various factors on the energy harvesting of piezoelectric Energy Harvesting Floor Tiles (EHFT) due to pedestrian traffic to supply power to micro-electronic devices and to set up energy harvesting specifications. The fatigue life of piezoelectric transducers under traffic loads was tested by Wang et al. [24], and a degradation rate of 32.37% was calculated after 10 million cyclic loads, illustrating that the life of piezoelectric transducers was longer than that of batteries. Yang et al. [25] tested the fatigue life of a PEH system by means of a one-third-scale accelerated test apparatus called The Model Mobile Load Simulator (MMLS1/3). The results showed that the proposed piezoelectric transducer was capable of resisting loads of up to 150 kN, fulfilling road traffic loads. Cao et al. [26] established two power output models that took into account moving loads and examined the relationship between vehicle loads and electrical energy outputs of a piezoelectric transducer. According to their study, it could serve as a reference for the design of piezoelectric transducers and road surfaces. Jeon et al. [27] designed a lever-type piezoelectric energy collector equipped with a deformation guide mechanism. For the energy storage experiment, after charging a 0.08 F capacitor to 5.09 V (1 J) in 170 min. Wang et al. [28] reported on a road piezoelectric micro-energy collection storage system. The energy conversion process has an

overall conversion efficiency of 26.8%, energy storage efficiency of 5.15%, and the 3300uF-based system is full-charged in 2~6 min. That is very important to piezoelectric energy collection technology. Liu et al. [29] examined the factors that influence Energy Harvesting Arrays (EHAs) in an experiment and explored the potential use of EHAs in traffic monitoring systems. Five factors were examined: the amplitude of loads, the cyclic frequencies of loads, the number of piezoelectric elements, temperature, and the composition of asphalt mixtures.

Contrary to previous works that concentrate only on single patch setups or laboratory-based vibration sources, this paper utilizes a multi-disc cantilever design directly attached to an actual vehicle engine head and also incorporates an energy management system via Raspberry Pi for battery charging and load delivery. In this study, a cantilever-based energy harvester was designed and fabricated with a strip of PZT-5A4E bimorph material. A mathematical model incorporating issues of frequency, amplitude, and material properties was used, and a set of simulations was carried out to predict performance. Experimental tests, with a beam fixed on an engine, showed good agreement with the analytical results, confirming that low-level engine vibrations can be converted into electrical energy using the proposed system (Figure 5).

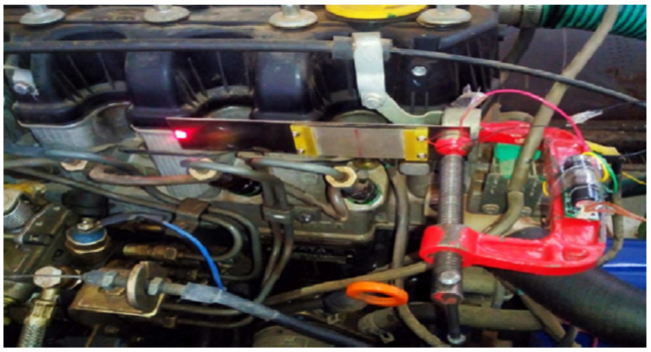

Figure 5. Piezoelectric cantilever beam mounted on the engine [22]

The vibration response of the beam was examined over an engine speed range of 750 to 2,400 rpm. The maximum deflection of 11 mm occurred at around 2,000 rpm, where the vibration amplitude of the engine was 2 mm. Peak response is due to the resonance effect, in which the natural frequency of the beam is aligned with the operating frequency of the engine [22].

Yet, recent studies have shown that multi-disc and hybrid piezoelectric arrangements can be very effective in improving charge accumulation and robustness, compared to single patch arrangements. The novelty of the work lies in the structural optimization achieved through the multi-disc PZT array and the spring-assisted vibration amplification, enabling improved strain distribution and stable voltage outputs during low-frequency engine vibrations, as described and validated via measurement on an actual engine head. The spring mechanism enhances the transmissibility of vibration; this is due to its ability to generate relative movement between the engine head and the cantilever, thus increasing the level of strain experienced by the cantilever beam resulting in improved energy conversion under resonance conditions.

3. Design and fabrication

3.1 *Components of energy harvester*

The Piezoelectric Energy Harvester (PEH) system consists of several significant components. These are piezoelectric patches and a cantilever beam, being the major energy harvesting components. The system also includes a bridge rectifier and an energy storage capacitor bank in the piezoelectric generator. Data acquisition and control make use of a Raspberry Pi, while voltage regulation is done by voltage converter. Moreover, mechanical components such as a C-clamp and springs ensure structural support and rigid mounting of the setup. The following components are to be designed: the cantilever beam, piezoelectric patches, and springs (Figure 6).

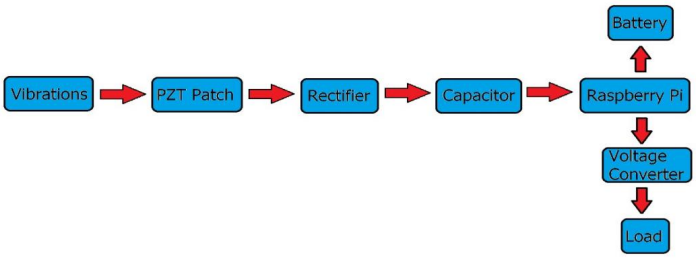

Figure 6. Complete flow diagram

3.2 *Circuit diagram*

The circuit of the system consists of 4 phases shown in Figure 7. These are as follows:

1. Electricity Generation
2. Rectification
3. Storage Control
4. Voltage Conversion and Load

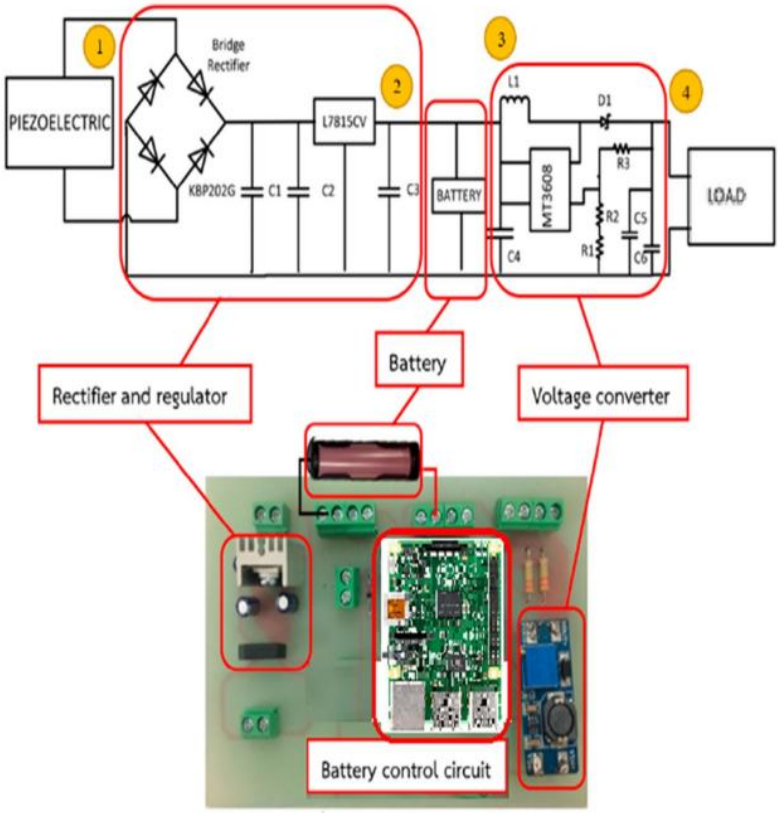

Figure 7. Circuit diagram of the system

The PZT patches in the 1st stage convert the vibrations to electricity. The use of a bridge rectifier in stage 2 will convert AC signals into pure or full wave DC signals that will be stored in the capacitor bank. Raspberry pi will be used as a battery control circuit in stage 3. The pi is programmed in such a way that it will distribute the generated electricity. The

principle behind its working is that when the battery is 90% complete, then the capacitor directly transfers the volt to the load connected and when the percentage of the battery is lower than the specified threshold, then first the capacitor charges the battery and then supply volt to the load. In the 4th stage, a voltage regulator was used to supply specific voltage to the components of the vehicle that require specific volts.

3.3 *Given standards and assumptions*

The engine considered in this study is a 4-cylinder type with a bore and stroke of 88 mm × 88 mm. The engine head has a length of 380 mm and a width of 70 mm. The assumptions made for this study include using a total of seven PZT patches and seven springs. The cantilever beam is considered to have a length of 450 mm, a width of 65 mm, and a thickness of 5 mm. Each PZT patch has a diameter of 35 mm and a thickness of 1 mm. The vehicle is assumed to be operating at 650 RPM with a speed of 50 km/h.

For cantilever beam, aluminum alloy 8011 is used because of its high flexibility, light weight and heat resistive properties. The length of aluminum beam is assumed to be 450 according to the standard dimensions of the engine.

The analytical power produced by piezoelectric generator is given by equation [30].

$$\text{Power Produced}(P) = \frac{\omega^2 b^2 h^2 e_{31}^2 \bar{A}\bar{A}R}{4\left(1+\frac{bL\varepsilon_{33}\omega R}{\Delta}\right)^2} \tag{1}$$

where; the symbol ω represents the frequency of the vibrating system, while b and h denote the width and thickness of the beam, respectively. In addition, e_{31} is the piezoelectric strain coefficient, with a value of 2.0817 C/m [31]. The deflection of the beam is denoted by $\overline{A}$, and R corresponds to the resistance applied to the electrical circuit. The diameter of the PZT layer is represented by L, On the other hand, $\varepsilon_{33} = 1,700 \times \varepsilon_r = 1,700 \times 8.85 \times 10^{-12}$ F/m was taken as the piezoelectric dielectric constant [31]. Finally, Δ denotes the thickness of the PZT layer.

The power produced by taking different widths of beam are as follows (Table 1, Figure 8):

Table 1. Relation between width of beam and power output

Width of Beam (mm)	Power output (μW)
25	552.97
30	795.63
35	1,082.1
40	1,412.2
45	1,785.81
50	2,202.92
55	2,663.37
60	3,167.06
65	3,713.88
70	4,303.73

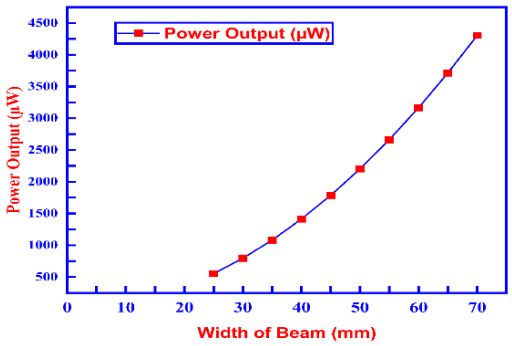

Figure 8. Graph between width of beam vs power output

Considering these values and knowing that the standard width of engine head is 70 mm, we chose the width of beam as 65 mm. Though a wider beam increased power, a width of 65 mm has been chosen considering a trade-off between electric performance and easy incorporation of engine-head. This is because wider beams had a tendency to become more rigid with a tight engine-head mounting constraint in the engine compartment.

The power produced by taking different thicknesses of beam is given below (Table 2, Figure 9) :

Table 2. Relation between thickness of beam and power output

Thickness of Beam (mm)	Power output (μW)
1	148.56
1.5	334.25
2	594.22
2.5	928.47
3	1,337
3.5	1,819.8
4	2,376.9
4.5	3,008.2
5	3,713.9

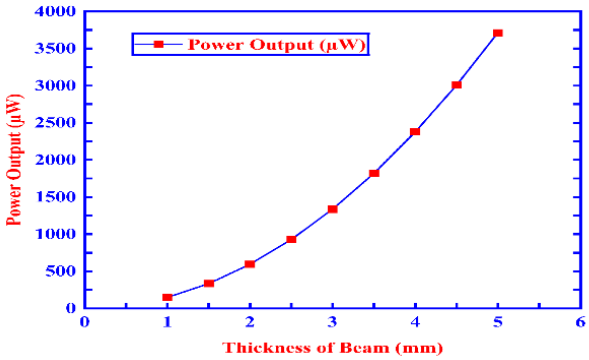

Figure 9. Graph between thickness of beam vs power output

Considering these values, we selected the thickness of beam as 5 mm.

The material that we have used for generating electricity is “Piezoceramic PZT-5A” due to the fact that it has high impedance, high sensitivity and high stability at elevated temperatures [32]. The power produced by piezoelectric depends upon diameter of the PZT layer. The power produced by piezoelectric depends on the thickness of the PZT layer. Therefore, referring to the equation of power produced, calculations were done based on different thicknesses of piezoelectric as follows (Table 3):

Table 3. Relation between thickness of PZT and power

Thickness of PZT (mm)	Power (μW)
1	3,599.2
1.5	3,549.5
2	3,675
2.5	3,690.5
3	3,700.9
3.5	3,708.3
4	3,713.9
4.5	3,718.2
5	3,721.7
5.5	3,724.6
6	3,727

So, based on the equation of power produced, we did calculations based on different lengths of piezoelectric, which is as follows (Figure 10):

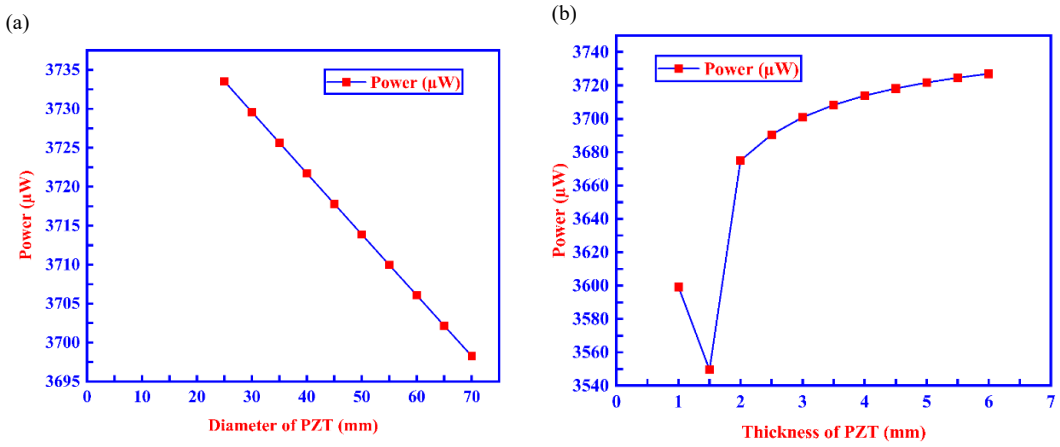

Figure 10. (a) Graph between diameter of PZT vs power output; (b) Relation of thickness of PZT vs power output

Considering these calculations and diameters of beam, we selected the diameter of PZT layer as 35 mm. Considering these calculations, we select the thickness of PZT layer as:

$$\text{Thickness of PZT layer} = 1 \text{ mm}. \tag{2}$$

For the spring design, the following standards are assumed. The material selected is Stainless Steel 302, conforming to ASTM A313 specifications. The spring has a wire diameter d of 1 mm and an outer diameter D_{out} of 15 mm. Its free length L_{free} is 25.4 mm, with 10 active coils n_{a} and a total of 12 coils n_{t}.

$$k = \frac{GD^4}{8D^3 n_a} \tag{3}$$

where; k is the spring constant, G is the shear modulus (75,000 MPa), d is the wire diameter, and D is the mean diameter of the spring, calculated as $D_{\text{out}} - d = 15 - 1 = 14$ mm. So,

$$\text{k} = \frac{75000(1)^4}{8(14)^3(10)} = 342 \text{ N/m}. \tag{4}$$

Coil pitch of spring is given by equation [33].

$$\text{Coil Pitch } = \frac{L_{\text{free}}}{n_a} = \frac{25.4}{10} \tag{5}$$

$$\text{Coil Pitch} = 2.54 \text{ mm}. \tag{6}$$

Solid height of the spring is given by equation [33].

$$L_{\text{solid}} = n_t \text{ d} = (12)(1) = 12 \text{ mm}. \tag{7}$$

Rise angle of the spring is given by equation [33].

$$\theta = \arctan\left(\frac{\text{coil pitch}}{\pi D}\right) = \arctan\left(\frac{2.54}{(3.14)(14)}\right) \tag{8}$$

$$\theta = 3.3^\circ. \tag{9}$$

3.3.1 *Calculations*

The system parameters used in the analysis are based on the following given data. The beam has a total length of 450 mm, with a width b of 65 mm and a thickness h of 5 mm. The piezoelectric (PZT) patch attached to the beam has a diameter L of 35 mm and a thickness Δ of 1 mm. Additionally, an external resistance R of 40 kΩ is connected in the electrical circuit.

We assume the following data:

• The amount of deflection produced in the cantilever beam is equal to the amount of deflection produced in springs attached on the beam.

• The car is running within 750 to 3,000 RPMs.

First, we have calculated the force which is exerted by the vibrations of a car engine running at 750 rpm.

The first frequency produced by 750 rpm:

$$\omega = \frac{RPM}{60} = \frac{750}{60} \tag{10}$$

$$\omega = 12.5\text{Hz}. \tag{11}$$

The natural frequency of the system is given by equation [30].

$$\omega = \sqrt{\frac{k}{m}} \tag{12}$$

Where, k is the stiffness of the spring and m is the mass of the vibrations. The stiffness is calculated above using equation (2); 342 $\frac{N}{m}$. Since, we have used seven springs in parallel. So, their equivalent stiffness will be:

$$k_{\text{equ}} = 7\text{k} \tag{13}$$

$$= 7 \times 342 \tag{14}$$

$$= 2394 \frac{\text{N}}{\text{mm}}. \tag{15}$$

Now, put in equation (12), it will give:

$$\omega^2 = \frac{k}{m} \tag{16}$$

$$\text{m} = \frac{k}{\omega^2} \tag{17}$$

$$\text{m} = 15.3216\ \text{kg}. \tag{18}$$

Since, Force is due to gravity, which is equal to weight, given by:

$$\text{F} = \text{W} = \text{mg}. \tag{19}$$

Substituting the value of m in equation (19), we get:

$$F = (15.3216)(9.81) \tag{20}$$

$$F = 150.305 \text{ N}. \tag{21}$$

The deflection of the spring is calculated using Hooke's law in equation [34].

$$F = kx \tag{22}$$

Rearranging equation (22)

$$x = \bar{A} = \frac{F}{k}. \tag{23}$$

Putting values, we get:

$$\bar{A} = \frac{150.305}{2394} \tag{24}$$

$$\bar{A} = 0.06278 \text{ m}. \tag{25}$$

Power is calculated using the power output equation, which is:

$$\text{Power Produced (P)} = \frac{\omega^2 b^2 h^2 e_{31}^2 A^{-2} R}{4\left(1 + \frac{bL\varepsilon_{33}\omega R}{\Delta}\right)^2}. \tag{26}$$

Substituting values, we get:

$$P = \frac{(12.7)^2\left(65 \times 10^{-3}\right)^2\left(5 \times 10^{-3}\right)^2 (2.0817)^2 (0.06278)^2 (40000)}{4\left(1 + \frac{(65\times10^{-3})(35\times10^{-3})(1700\times8.85\times10^{-12})(12.7)(40000)}{(1\times10^{-3})}\right)^2}, \tag{27}$$

$$P = 0.002794 \text{ W} = 2875 \times 10^{-6}, \tag{28}$$

$$P = 2875\ \mu\text{W}. \tag{29}$$

The output voltage is calculated using the ohm's law which is given by equation

$$V = IR. \tag{30}$$

Where I is the current, V is the voltage and R is the resistance. We have another power, voltage and current relation given by equation

$$P = VI. \tag{31}$$

Where P is the power output. Solving for I from both equations, we get:

$$\frac{V}{R} = \frac{P}{V}. \tag{32}$$

Solving for voltage (V), we get:

$$V = \sqrt{PR}. \tag{33}$$

Substituting values, we get:

$$V = \sqrt{(2794 \times 10^{-6})(40000)} = 10.572 \text{ V}. \tag{34}$$

3.3.2 *Comparison*

We have calculated power and voltage output on varying RPMs from 750-3,000. The results are presented in Table 4 and Figure 11:

Table 4. Relation between RPM and power output

RPM	Power	Voltage (V)
750	2,785	10.573
850	2,173.1	9.323
950	1,737.7	8.337
1,050	1,420.8	7.539
1,150	1,183.1	6.879
1,250	1,000.2	6.325
1,350	856.5	5.853
1,450	741.56	5.446
1,550	648.21	5.092
1,650	571.36	4.781
1,750	507.334	4.505
1,850	453.442	4.259
1,950	407.66	4.038
2,050	368.43	3.839

Table 4. (cont.)

RPM	Power	Voltage (V)
2,150	334.56	3.658
2,250	305.13	3.494
2,350	279.39	3.343
2,450	256.75	3.205
2,550	236.74	3.077
2,650	218.95	2.959
2,750	203.08	2.85
2,850	188.86	2.749
2,950	176.07	2.654
3,000	170.16	2.609

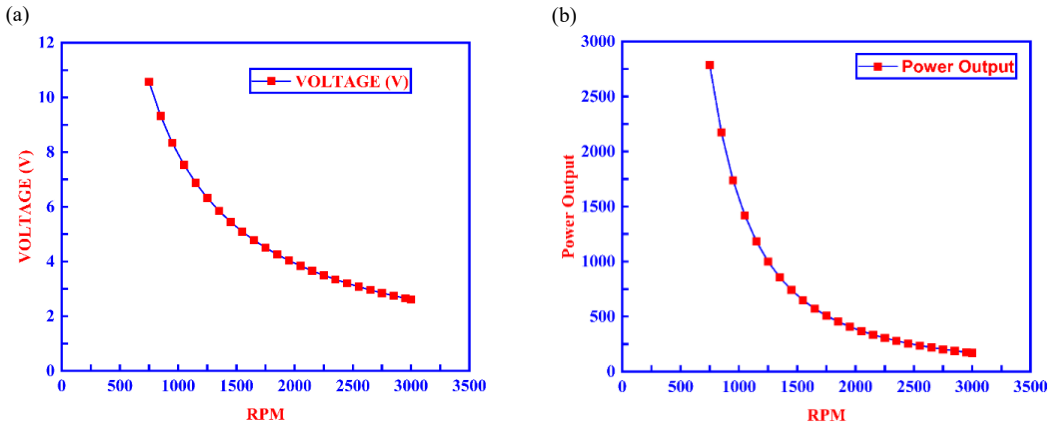

Figure 11. (a) Relation between RPM and voltage; (b) Relation between RPM and power output

3.4 *Modeling and fabrication*

Model of beam with springs and PZT discs is given in Figure 12 which contains 7 discs, 7 springs, mounted on the aluminum beam. A configuration of seven PZT discs was chosen after performing parametric simulation to investigate the effect of different numbers of PZT discs, ranging from 3 to 9. The results showed that using fewer than seven PZT discs resulted in a reduction of approximately 25% to 35% in output voltage, whereas using more than seven resulted in higher system stiffness, thus reducing cantilever tip deflection by approximately 18% to 22%.

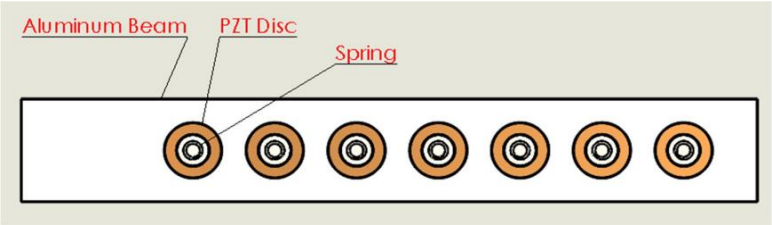

Figure 12. Model of system

The 2D views of Aluminum beam are shown in the Figure 13a. Figure 13b shows the 3D Model of beam.

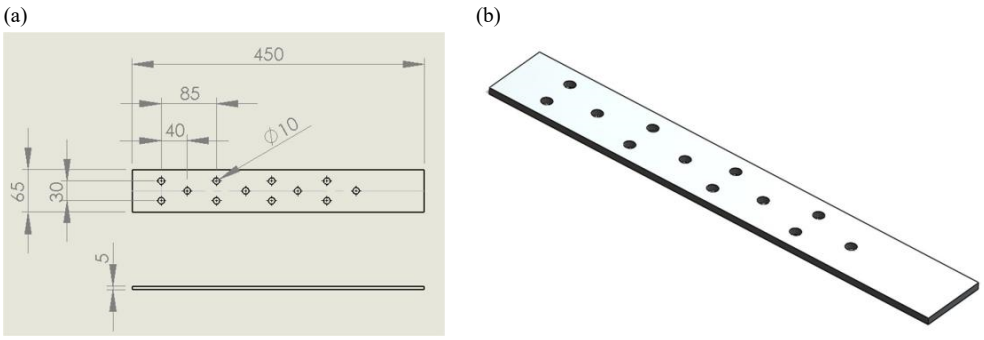

Figure 13. (a) 2D views of aluminum beam; (b) 3D model of aluminum beam

The detailed model of the spring used in the assembly is shown in Figure 14.

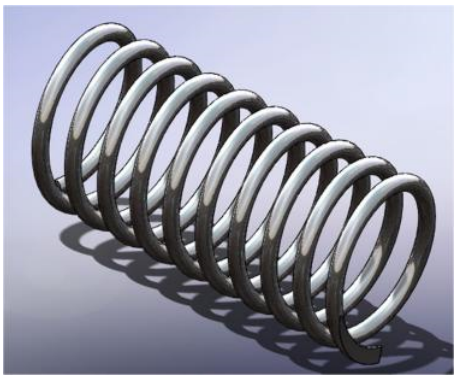

Figure 14. 3D model of spring

The top and side 2D views of the PZT layer are shown in Figure 15a. Figure 15b shows the 3D model of the PZT Layer where 1 mm thick PZT-5A material is bonded in between two copper electrodes.

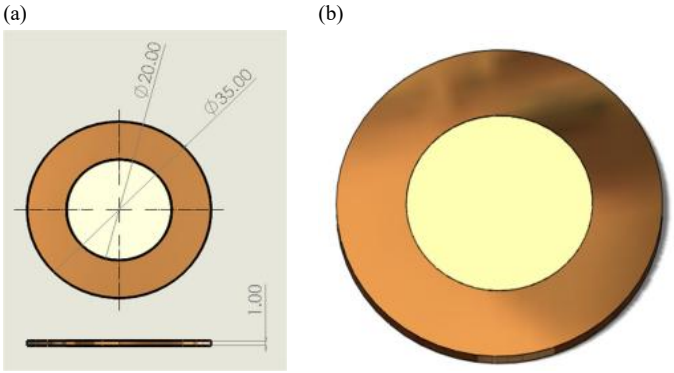

Figure 15. (a) 2D views of PZT layer; (b) 3D model of PZT layer

Complete 3D model of the system is given below (Figure 16):

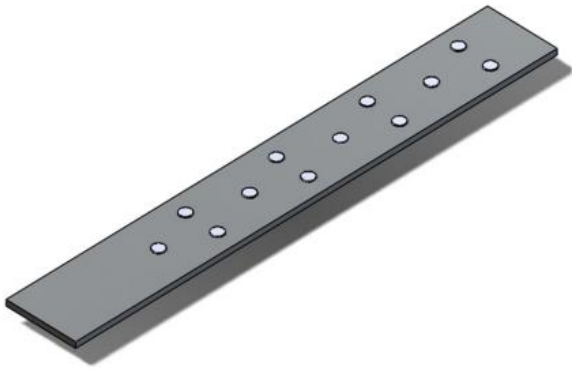

Figure 16. Complete model

The complete assembly of the beam, PZT discs, springs, and bolts is illustrated in Figure 17.

Figure 17. Complete assembly of beam, PZT, springs and bolt connections

Figure 18 shows the complete 3D assembly of the system consisting of an Aluminum Beam, Springs, PZT Layers and Bolts for connection purposes.

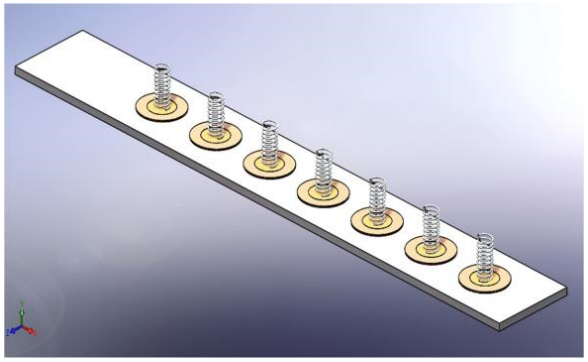

Figure 18. Complete 3D model

The entire system is installed on the engine head (Figure 19). The springs are placed on top of the engine head, and the beam is fixed on one side using a C-clamp. The complete setup is shown in Figure 20.

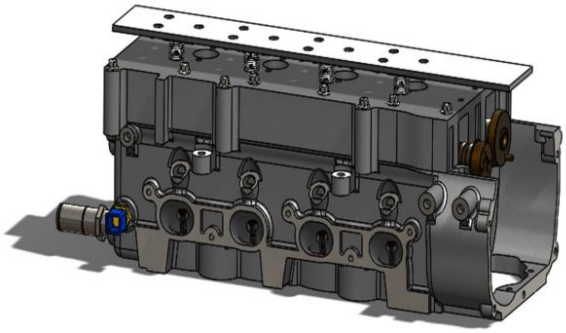

Figure 19. Beam mounted on engine head

Figure 20. Burnout process

Fabrication of Piezoelectric Energy Harvester involves the construction of all the major components as well as the collection of components that are to be assembled in order to complete the research. It covers the construction and manufacturing of all the necessary components to produce electricity from piezoelectric patches attached on a cantilever beam which is mounted on the vehicle's engine.

The fabrication of such a PEH system entails intricate design considerations, material selection, and manufacturing techniques to ensure optimal performance and durability under demanding automotive conditions.

We have fabricated the aluminum beam, piezoelectric patches and battery control circuit which helps in controlling the supply of produced voltages to the battery and load applied. The mounts of the system have been fabricated in such a way so it acts as a universal system, meaning that it can be mounted on any of the vehicle regardless of its type, shape and working.

3.4.1 *Properties of materials*

PEH System consists of different components having specific properties for achieving the desired output. These properties are as follows (Table 5):

Table 5. Components and materials properties

Sr. No.	Components	Materials	Properties	
1	Cantilever Beam	Aluminum Alloy 8011	Density [35]	2.71 g/cm^3
			Tensile Strength [36]	140 MPa
			Shear Modulus [36]	26 GPa
			Young's Modulus [36]	69 GPa
			Fatigue Strength [36]	33-76 MPa
			Thermal Conductivity [36]	237 W/mK
			Yield Strength [37]	110 MPa
2	PZT Patch	Lead Zircotitanete Ceramic ($PbZrO_3$-$PbTiO_3$)	Young's Modulus E_{11} [17]	5.8×10^{10} N/m^2
			Poisson Ratio μ [17]	0.35
			Relative Dielectric Constant ε_{33} [17]	1,700 ε_r
			Piezoelectric Constant ε_{31} [17]	2.0817 C/m^2
			Electro-Mechanical Coupling k_{31} [17]	0.35
			Static Capacitance C [17]	30 nF
3	Spring	Sainless Steel 302 ASTM A313	Young's Modulus	193 GPa
			Shear Modulus	75 GPa
			Tensile Strength	1,345 MPa
			Poisson's Ratio	0.25

The specifications of the various parts used in this research are outlined as follows. The cantilever beam is made of Aluminum Alloy 8011 with dimensions of 450 mm in length, 65 mm in width, and 5 mm in thickness. The piezoelectric patches are made of Piezoceramic PZT-5A, disk-shaped with a diameter of 35% ± 2% mm and a thickness of 1 mm, with a total of seven patches used. The spring is fabricated from Stainless Steel 302 ASTM A313, having an outer diameter of 15 mm, a free length of 25.4 mm, 12 total coils with 10 active coils, a stiffness of 342 N/m, a coil pitch of 2.54 mm, and a rise angle of 3.3°. The Raspberry Pi used is the Raspberry Pi 4 B model with 4 GB RAM and 16 GB ROM, powered via USB C-type at 5.1 V and 3 A.

3.4.2 *Working of parts*

Cantilever beam is one of the most important components of the system. A cantilever beam is used to hold all the components into one place, we can say it is the house of all other components. It consists of piezoelectric patches and their attachments, springs bonded on patches, and all the other electronics needed for power generation like capacitors, resistors, raspberry pi and all the wirings. Piezoelectric Patch is the second main component of the system. It produces electricity when mechanical stresses; vibrations, are applied on it. Seven number of piezoelectric patches are used in parallel configuration. These are attached on the cantilever beam using steel epoxy. The choice of the PZT discs is a compromise among the voltage increase, mechanical loading, and stiffness of the beam. Initial experiments showed that above a certain number of discs, say above seven, the mass of the system increases and the deflection of the beam decreases, and below the voltage levels are lower. Hence, the choice of the discs is optimal. Springs are used to aid the vibrations produced in vehicle's engine. These are attached on the surface of piezoelectric patch. When the engine vibrates, the springs aid in these vibrations and transfer the vibrations in high amplitude to the piezoelectric patches, which further convert these vibrations into electricity, mainly Direct Current (DC). Raspberry pi acts as a battery control unit, which is a microcontroller in this system. It is programmed in such a way so as to distribute the generated electricity. The cut-off point of 90% of battery charge was adopted to prevent the battery from charging to full capacity while maximizing the utilization of the energy. Beyond the cut-off point, the surplus charge goes to the load to reduce the strain on the battery. Bridge rectifier is used to convert the Alternating Current (AC) to Direct Current (DC). Since the current produced by converting vibrations through piezoelectric patches is alternating current. So, in order to use this current in the vehicle, we

have to convert it into Direct Current. So, the bridge rectifier is used. Since, there are different components in the vehicle having different operating voltages such as 3 V, 5 V, 6 V, 9 V and 12 V. So, to operate these components, voltage regulator is used to provide specific voltage to these components to provide safe operations and to avoid the risk of burnout of the component.

3.4.3 *Fabrication of parts*

Different processes and operations performed for the manufacturing of different components. The fabrication of piezoelectric patch consists of following processes:

1. Pressing.
2. Burnout (1st stage).
3. Electrodes.
4. Oven Dry.
5. Burnout (2nd stage).
6. Poling.

3.4.3.1 *Pressing*

First process in the manufacturing of PZT patches is pressing of the piezoelectric material in the desired shape, disk shape in this case. A small amount of PZT-5A material is taken and mixed with binder in order to keep the material in place and then the mixture is inserted in the die and pressed, it is then shaped into the disk cavity of the die (Figure 21).

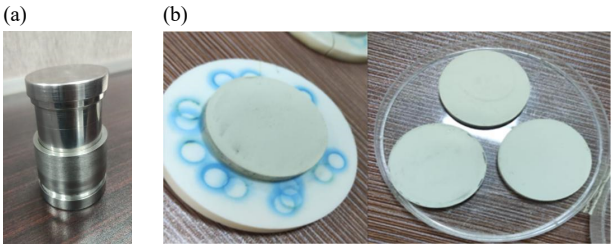

Figure 21. (a) PZT disk die; (b) Patches after pressing

3.4.3.2 *Burnout (1st Stage)*

Second step is the burnout of mixture. Since, there is binder in the material. So, it is removed using "Box Furnace". The mixture is kept in the box furnace for a complete profile of different temperatures and for different durations. The burnout is done on 780 °C. The complete profile of burnout is given in Table 6.

Table 6. Burnout profile

Temperatures	Duration
Room temp.—150 °C	1 hour 30 minutes
120 °C–250 °C	1 hour
Hold	1 hour 30 minutes
250 °C–300 °C	30 minutes
300 °C–400 °C	1 hour
400 °C–600 °C	2 hours
600 °C–780 °C	2 hours
Hold	2 hours

3.4.3.3 *Sintering*

It is the third step in fabrication of piezoelectric discs. It involves heating and removal of extra binder which remained after the burnout process. This process is also done in "Box Furnace" and complete profile of different temperatures and different durations is maintained for complete sintering of the PZT disc. The sintering profile of the PZT disc is shown in Table 7. The sintering and poling conditions were chosen following typical process requirements for PZT-5A ceramics as described in the literature, to ensure a reliable ferroelectric domain structure.

Table 7. Sintering profile

Temperatures	Duration
Room temp.—120 °C	1 hour 40 minutes
120 °C–250 °C	2 hours 10 minutes
250 °C–900 °C	9 hours 30 minutes
900 °C–1100 °C	2 hours
1100 °C–1280 °C	2 hours 15 minutes
Hold	4 hours

3.4.3.4 *Poling*

It is the process of aligning the electric dipoles in the material's crystal to enable the material's piezoelectric properties. In this process a high DC voltage is applied to the material under specific temperature for specific time period. We have applied 2,000 volts per mm of component thickness for the poling. Figure 22 shows the representation of aligned domain, during and after the poling process. Left shows the poling process during application of DC voltage and right shows the results of poling after the removal of voltage.

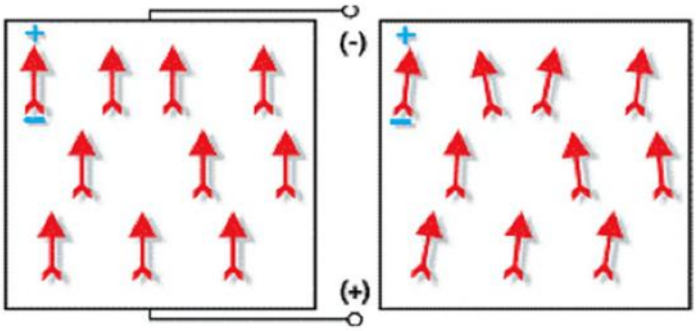

Figure 22. Alignment of electric dipoles

3.4.4 *Completed fabricated PZT disc*

After the poling process is completed, the PZT discs are again passed through same burnout cycle for further drying of the mixture and removing the remaining binder. Figure 23 shows the complete fabricated PZT disc.

Figure 23. Piezoelectric discs

Cantilever beam of aluminum alloy is cut using circular saw cutter. Firstly, aluminum beam is firmly clamped to a desk and marked a line on the sheet. Then, adjust the cutting saw to the depth of beam and slowly move the cutter to a length desired apply gentle pressure. Manufacturing of the spring is conducted by wire forming process. In this process, it is shaped into a coil form using wire forming machine. This coil is now then coiled around a mandrel to achieve the desired shape and dimension.

3.5 *Assembling processes*

Assembling process involves the assembly of all the fabricated as well as purchased parts. Firstly, we assembled the PZT discs in their covering which creates a gap between the beam and PZT disc to get deflections, instead of directly fixing the PZT on the beam. The springs are joined on the top surface of the PZT to get extra vibrations. The cover of the PZT is bonded on the beam using steel epoxy and springs are also bonded to PZT surface using epoxy. Figure 24a shows the cantilever beam with springs and PZT discs covered and bonded with steel epoxy.

Secondly, seven full bridge rectifiers are made using 4 diodes. Since, we have used 7 PZT disc, so 7 rectifiers are connected to each disc in parallel circuit to enhance the voltage and final output is obtained by combining the outputs of all the rectifiers into single output. The number of PZT disks was decided depending on available surface area, strain distribution on the cantilever, and electrical interconnections. Seven disks were found to provide a good distribution for the high-strain areas without causing electrical loading or stiffness to the cantilever beam. Beyond this number, the returns become diminishing due to the effects of strain dilution, among other factors. Figure 24b shows the bridge rectifier.

Figure 24. (a) Beam with PZT discs; (b) Bridge rectifier

Thirdly, we created a charging and discharging circuit for the battery using raspberry pi 4. Two LEDs are used to show the charging and discharging of the battery and LCD is used to display the status of battery. All the setup is shown in Figure 25a and is enclosed in box containing neon LED strip, which is used for discharging of the battery and live load for the piezoelectric generator.

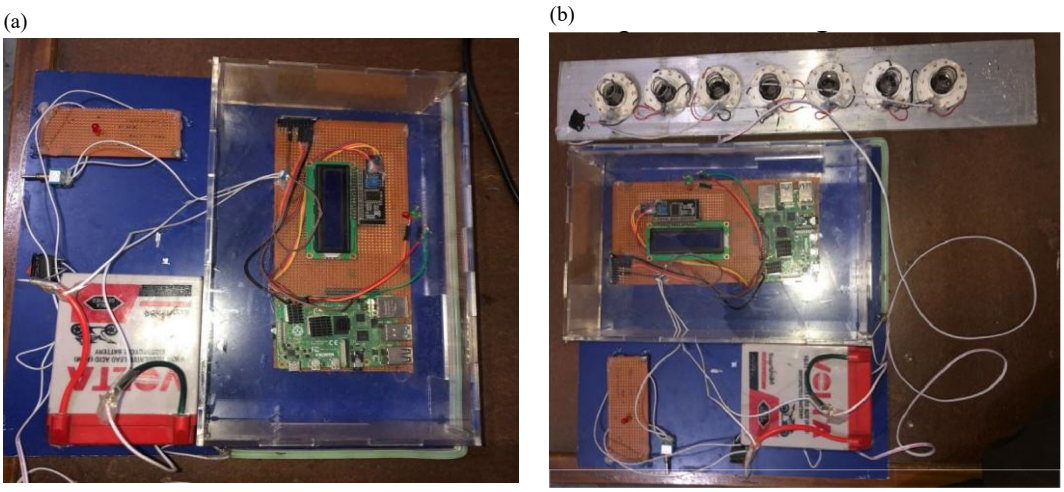

Figure 25. (a) Charging discharging circuit; (b) Complete fabricated circuit

3.6 *Programming*

The programming for this research was carried out on a Raspberry Pi 4 using the Debian desktop operating system. For the setup, an SD card was inserted into the Raspberry Pi, and the Debian OS for desktop was downloaded and installed. The coding was performed in Python language using the Thonny IDE, which is the built-in software of the Raspberry Pi. The program was designed to configure the Raspberry Pi to monitor the voltage of a 12V battery and display its charge percentage on an LED display. An MCP3008 ADC was used to read the analog voltage from a voltage divider circuit that scaled down the 12V to a readable range for the Raspberry Pi. The acquired voltage data was then used to calculate the battery's charge percentage, which was displayed through an LED display via the I2C protocol. The code was written to continuously monitor the voltage and update the display every second, ensuring real-time monitoring of the battery status.

4. Results and discussion

Experimental phase involves the practical application of the research through testing and experimentation to gather data and validate concepts. This phase is crucial to compare the theoretical results with the real-life experiments. We mounted the system on four-cylinder petrol engine vehicle's head and setup all the electronics at the front dashboard of the car. Then we tested the system for static vehicle as well as running the vehicle at several rpms.

4.1 *Setup*

The experiments are setup by placing the cantilever beam which has PZT discs fixed on its surface, on the vehicle's engine head. The wires are kept lengthy so as to verify the output readings while running the vehicle at different rpms. The control box or circuit box is placed on the front dashboard of the car. LED display is used to observe the battery status while charging and discharging. Discharging of the battery is done by neon LED fixed outside the box. The output voltage is measured using voltmeter. The piezoelectric beam fixed on engine's head is shown in Figure 26a, while the control/circuit box placed on front dashboard of the car is shown in Figure 27.

(a)

(b)

Figure 26. (a) Cantilever beam mounted on engine's head; (b) Clamped beam on engine's head

Figure 27. Control box on front dashboard

4.2 *Results*

The vehicle's rpms were recorded by vehicle's meter reading and the output voltage is measured by voltmeter. The battery status was observed on LED display on the control box. It was observed that the battery status increased when the car was just started and decreased when the external load (i.e., neon LED on board) is applied. But when the car gains some rpms from 500 to 1,500, the battery status increased, it is because the voltage was generated continuously from the piezoelectric generator. The voltmeter readings are observed and recorded in the Table 8 and Figure 28 shows the relationship between output voltage and rpm of the vehicle.

Table 8. Relationship between RPM and output voltage

Sr. No.	Revolutions per Minutes	Output Voltage (V)
1	500	14.510
2	750	9.471
3	1,000	7.148
4	1,250	6.691
5	1,500	5.172

Theoretical range of RPM, falling between 750-3,000 RPM, represents the generalized dynamic capability of the system. However, experimental validation was restricted to 500-1,500 RPM due to constraints imposed regarding the safety

of engine operation, stable operation, and the reliability of measurement. The experimentally verified RPM range fully covers urban driving situations where a voltage level (5.17-14.51 V) and power output are achieved within the milliwatt range. The electrical output presented is that for the average power that can be calculated on account of measurements taken for the RMS voltage being applied to a resistive matching load when it is in a state of steady-state vibration. Also, peak values for voltage are given to present an understanding of transient response conditions to resonance.

$$P_{avg} = \frac{V_{RMS}^2}{R}. \tag{35}$$

The reduction in voltage with increasing engine speed is said to occur due to off-resonance excitation of the cantilever beam. As the RPM increases, the voltage-excitation frequencies move away from the fundamental natural frequency of the cantilever beam, thus decreasing the amplitude of vibrations. Moreover, damping and impedance also increase with a rise in voltage-excitation frequencies. When the frequency of the engine excitation passes the system's first resonant frequency, the amplitude of the vibrations of the beam will reduce, thus reducing the strain and the piezoelectric voltage. An experimental comparison shows the factor of amplification of vibration amplitude near resonance to be about 1.4 to 1.6 times, resulting in higher energy conversion in the electromagnetic field. The amplifying factor was found through the measurement of the peak cantilever tip movement and associated voltage output difference when the spring was introduced, compared to measurements when the spring was absent. There was a corresponding increase of 40%-60%, or 1.4-1.6 times.

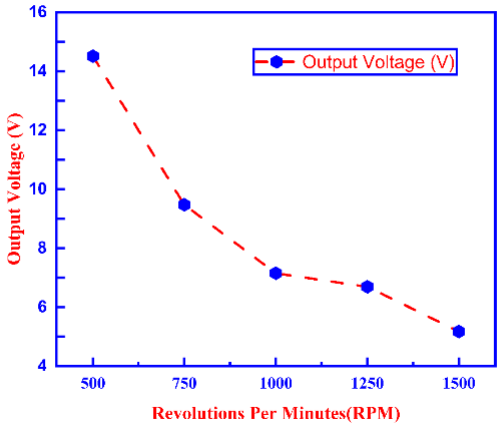

Figure 28. Relation between output voltage and RPM

4.3 *Software analysis*

FEA is more advanced approach to predict the dynamic response of piezoelectric cantilever beam generator as compared to traditional analytical approach. The FEA simulation is performed on ANSYS Workbench and is compared with experimental results. Followings are the steps taken for FEA simulation:

4.3.1 *Pre-processing*

Pre-processing involves the material selection for the analysis. Since ANSYS 2023 version is used for the analysis, it contains built-in piezoelectric materials library from which, we selected PZT-5A material for PZT discs and Aluminum Alloy for cantilever beam from general materials. The material selection from the Engineering Data Sources in ANSYS is shown in Figure 29.

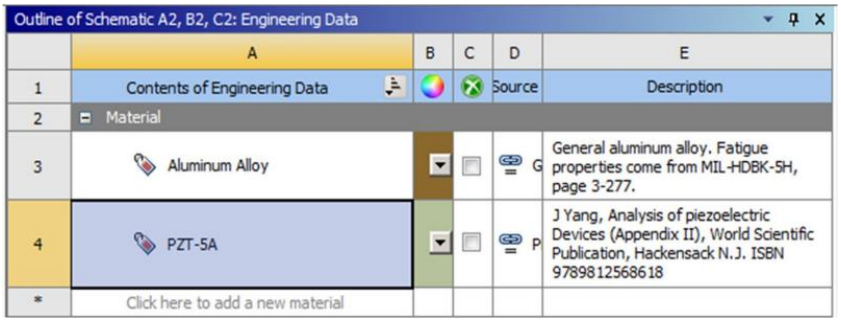

Figure 29. Material selection

Then Piezo & MEMS extension shown in Figure 30, is downloaded from Ansys store and loaded into the ANSYS 2023 and enabled. This extension is used to enable piezoelectric properties in the geometry and also used to explore the piezoelectric results such as voltage, electric potential, and electric flux etc.

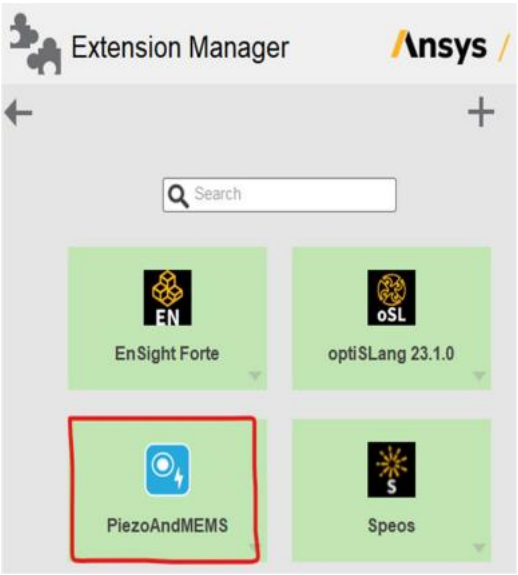

Figure 30. Piezo and MEMS extension

Then from ANSYS Workbench, geometry is selected and opened in Design Modeler. A cantilever beam with dimensions specified was modelled along with PZT disc patches as shown in Figure 31 and materials are assigned to each part.

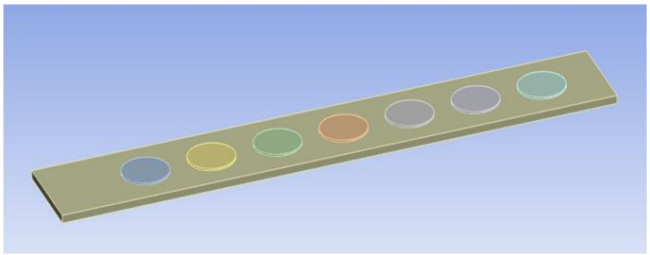

Figure 31. Modeling of system

4.3.2 *Modal analysis*

After the pre-processing step, modal analysis of the system is done in order to find the natural frequencies of the system up to 3 mode shapes for cantilever beam and their respective tip displacements are calculated. The beam is fixed at one end. Figures 32-34 show the three shape modes obtained with the natural frequencies of 23.227 Hz, 146.73 Hz and 279.61 Hz, with the tip displacements of 3.0434 mm, 3.1221 mm and 3.0454 mm respectively.

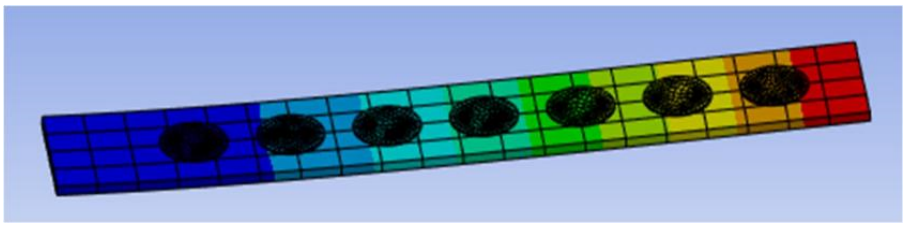

Figure 32. First mode shape

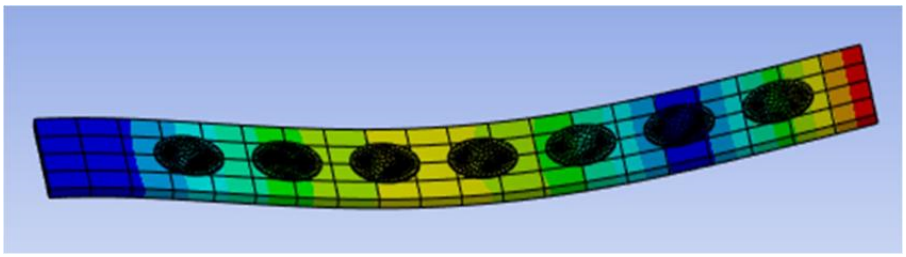

Figure 33. Second mode shape

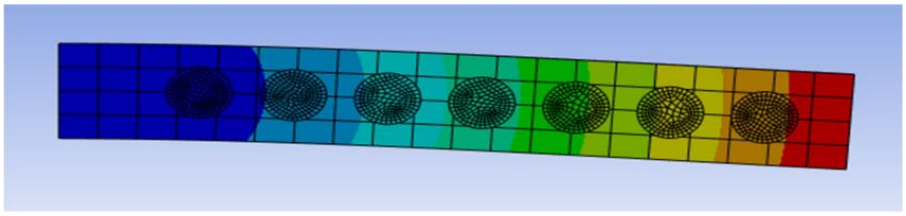

Figure 34. Third mode shape

4.3.3 *Harmonic response analysis*

Harmonic analysis was performed using the natural frequencies obtained from the modal analysis. In this analysis, an acceleration of 2 m/s^2 was applied to represent the vibrations produced by the vehicle's engine. A piezoelectric body was added to the model, and all seven PZT discs were selected, with their top surfaces set to ground (zero voltage). The analysis was carried out for frequencies ranging from 0 to 300 Hz. As shown in Figure 35a, the amplitude decreases as the frequency increases. Figure 35b shows the phase response of the system which is sine wave, it means that AC voltage is generated.

The voltage output for 16.67 Hz frequency (i.e., 1,000 RPM) is 7.3236 V as seen in Figure 36, which is close to the analytical approach value i.e., 7.918 V.

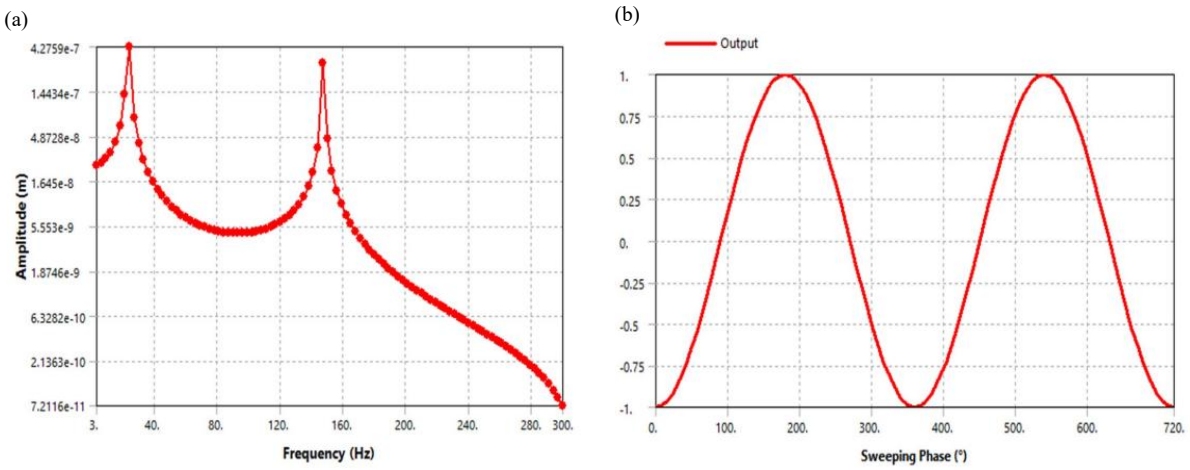

Figure 35. (a) Relation between frequency and amplitude; (b) Phase response of system

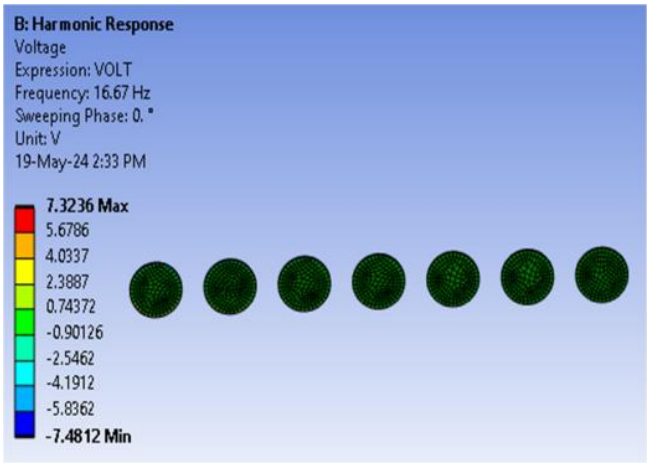

Figure 36. Output voltage of the system

4.3.4 *Static structural analysis*

Finally, the static structural analysis is done to calculate voltage and displacement response by changing the acceleration of the vibrations. The results are shown in Table 9 and Figure 37. It is noticed from results that increasing the acceleration of the vibrations, displacement of the tip of beam increases and as a result, voltage increases.

Table 9. (a) Relation between beam deflection and acceleration of vibrations; (b) Relation between output voltage and acceleration of vibrations; (c) Relation between beam deflection, output voltage and acceleration of vibrations

Steps	Time [s]	[A] Acceleration [m/s^2]	[C] Total Deformation (Max) [m]	[E] Voltage (Max) [V]
1	1	1	7.2683×10^{-5}	1.7177
2	2	3	2.1805×10^{-4}	5.1531
3	3	4	2.9073×10^{-4}	6.8707
4	4	7	5.0878×10^{-4}	12.024
5	5	9	6.5415×10^{-4}	15.459

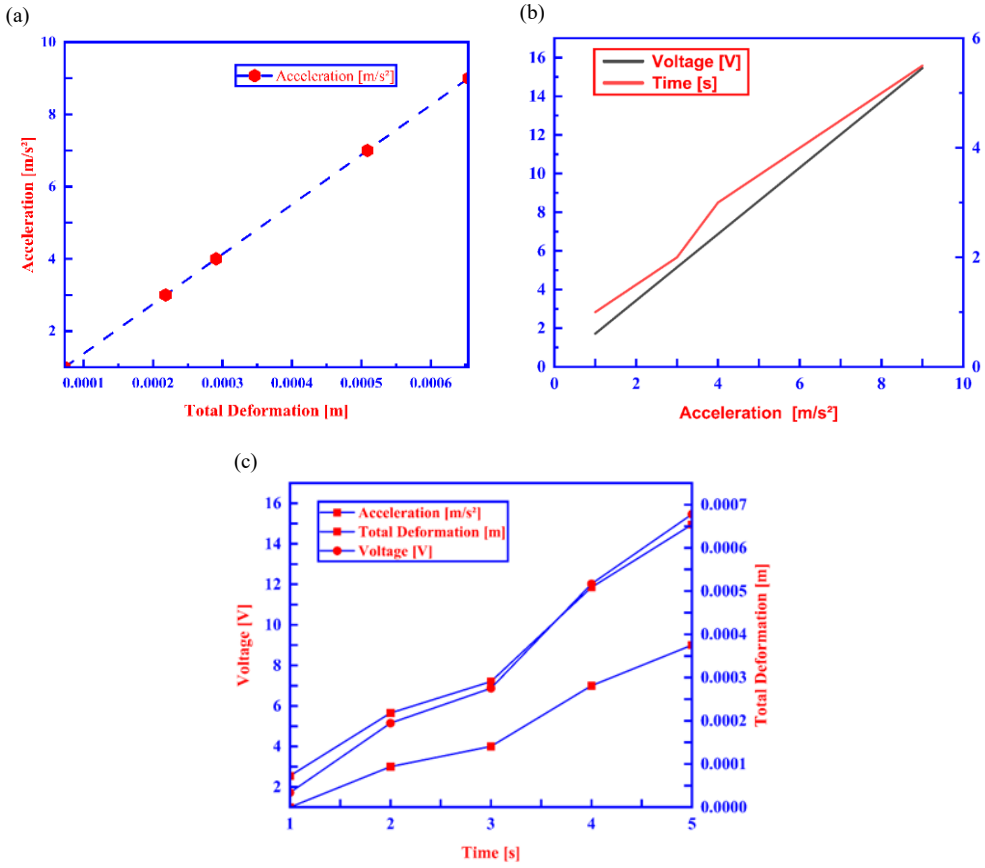

Figure 37. (a) Relation between beam deflection and acceleration of vibrations; (b) Relation between output voltage and acceleration of vibrations; (c) Relation between beam deflection, output voltage and acceleration of vibrations

It is seen that if the displacement is 0.2907 m, then the output voltage is 6.87 V and when we compare this result with the analytical results, we obtained 7.19 V at that displacement. Hence, both the results are in close match. The complete schematic is shown in Figure 38.

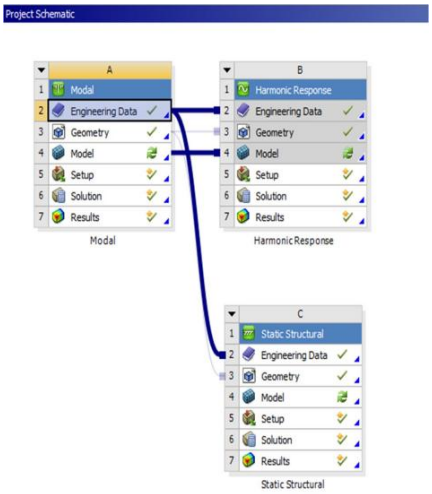

Figure 38. Complete schematic

A coupled deformation and piezoelectric problem is considered in a Finite Element Model using the Piezo & MEMS module in ANSYS. Experimental voltage data taken under the same vibration frequency was verified to match simulation data.

4.4 *Reference model*

The reference model is given in Figure 4. It consists of an aluminum cantilever beam with piezo mounted at 282 mm from the fixed end. The material used for piezo is PZT-5A. A rectangular shaped PZT-5A having length 64 mm, width 32 mm and thickness of 0.16 mm was used. It is noted that at 850 rpm, the maximum voltage is generated which is 4.1 volts.

4.5 *Comparison of reference model with our model*

The new system shows better voltage generation compared to the most recent piezoelectric harvester designs that have been described in the literature. The system to be designed highlights integration simplicity and robust structure. Unlike designs that involve suspension systems or hybrid designs, the currently designed system focuses on the aspect of integration. We have compared the results of our model with the reference model and it seems that there is a great enhancement in our model. The output voltage of the reference model at 850 rpm was 4.1 volts, while our model generated output voltage of 9.32 volts at same rpms. There is much difference of the generation and our model seem to be much efficient as compared to the reference model (Table 10).

Table 10. Comparison of reference model with our model

Revolutions per Minutes	Output Voltage (V)		Difference (V)
	Reference Model	Our Model	
850	4.1	9.32	5.22

The better performance of the proposed model is largely due to the multi-disc piezoelectric arrangement, which results in more charge being generated, as well as the optimized geometry of the cantilever, which improves the strain distribution. In contrast to the reference model which uses one rectangular patch, the proposed uses a set of disc-shaped PZT patches, which result in more voltage being generated.

In conclusion, the experimental and simulation results clearly illustrate that the proposed energy harvester operates effectively in practical engine vibration conditions. Even though it may not operate at the highest RPM for resonance conditions, it ensures stable voltage output within a wide range of operation.

5. Conclusion and future recommendations

We have designed and fabricated the piezoelectric energy harvester for smart vehicles, which consists of an aluminum cantilever beam of length 450 mm, width 65 mm and thickness 5 mm, and seven piezoelectric discs of 35 mm diameter and 1 mm thickness having material Lead Zirconate Titanate (PZT-5A). The system was clamped on the four cylinders petrol vehicle's engine head. The experiments were done for running the vehicle from 500 to 1,500 rpms and output voltage was measured. The experiments show that 14.51 volts are generated at 500 rpm and goes on decreasing as rpm increases and the least measured voltage of 5.172 V is observed at 1,500 rpm. From the measured voltage reading and load resistance value, the approximate output power rating is estimated to be around milliwatt levels, which is ideal for low-powered sensors, sensors used for monitoring, wireless modules, auxiliary lighting systems or secondary electronics used in vehicles. The work that is presented in the current study involves steady-state engine operations. Additionally, future research may include studies of transient driving cycles, durability, as well as miniaturization. Cost-effectiveness of integration as well as reliability when subjected to long durations of vibration could be important factors. Good resistance

to fatigue under cyclic loading is ensured by the use of PZT-5A material and stainless-steel springs. No degradation of the mechanical system was observed during the testing process. An assessment of the long-term system durability through the use of the cyclic vibrations process is recommended for future studies.

Some of the suggestions or proposals for the future regarding this research:

• Invest in research to ascertain and develop new piezoelectric materials that are more efficient and have longer lifetimes.

• Research the use of nanomaterials and nanostructures to improve the performance and efficiency of piezoelectric devices.

• Develop methods to integrate piezoelectric harvesters efficiently into various components of a vehicle, i.e., suspensions, tires, and engine mounts.

• Design high-performance energy management systems with the ability to store and utilize the harvested energy effectively, maintaining maximum utilization in the vehicle's electrical network.

• Focus on reducing piezoelectric harvester manufacturing costs through scalable production processes and low-cost materials.

• Establish manufacturing processes to mass-produce piezoelectric energy harvesters with quality and reliability assurance.

• Collaborate with automobile manufacturers to design vehicles that are designed for integration of PEH technologies right from the start.

• Retrofit kits for current vehicles to be easily fitted with PEH systems; this will increase market penetration and impact.

• Encourage the installation of smart roadways and infrastructure that are capable of communicating with vehicles incorporating piezoelectric harvesters, making overall efficiency in transport networks improved.

• Integrate the piezoelectric energy harvesters into bigger systems of energy storage and smart grid for maximum utilization and potential.

• The proposed system relies on commonly available materials that use simple processing techniques and is thus suitable for miniature designs and mass production. The proposed system may also be integrated with engine mounts or compact housings to produce production vehicles with further optimizations.

In the future, various techniques to overcome the limitation of relying on the vibrations generated just by the engines would be explored by incorporating the harvester with vibrations from other parts of the vehicles, like the suspension system, wheel hubs, and tire road interface. Future work will be done to explore further research on harvesting hybrid vibrations, optimization, and tuning of devices for increased power density and practical application. These recommendations, if taken into consideration, could greatly advance the development and use of piezoelectric energy harvesters for smart cars in order to achieve sustainable transportation systems and innovation in general industry and infrastructure development.

Conflicts of interest

The authors declare no conflicts of interest.

References

[1] C. Jettanasen, P. Songsukthawan, and A. Ngaopitakkul, "Development of micro-mobility based on piezoelectric energy harvesting for smart city applications," *Sustainability*, vol. 12, no. 7, p. 2933, 2020. https://doi.org/10.3390/su12072933.

[2] M. Zhu, Z. Kuang, W. Liao, J. Zhang, L. Fu, Z. Zhang, et al., "A piezoelectric wind-induced vibration energy harvester via the venturi effect," *Applied Physics Letters*, vol. 126, no. 7, 2025. https://doi.org/10.1063/5.0249187.

[3] H. Liu, J. Zhong, C Lee, S.-W. Lee, and L. Lin, "A comprehensive review on piezoelectric energy harvesting technology: Materials, mechanisms, and applications," *Applied Physics Reviews*, vol. 5, no. 4, 2018. https://doi.org/10.1063/1.5074184.

[4] G. Pepe, A. Doria, N. Roveri, and A. Carcaterra, "Vibration energy harvesting for cars: Semi-active piezo controllers," *Archive of Applied Mechanics*, vol. 93, no. 2, pp. 663-685, 2023. https://doi.org/10.1007/s00419-022-02292-1.

[5] H. Jaffe and D. Berlincourt, "Piezoelectric transducer materials," *Proceedings of the IEEE*, vol. 53, no. 10, pp. 1372-1386, 1965. https://doi.org/10.1109/PROC.1965.4253.

[6] P. P. Braz, "Design of piezoelectric devices for simultaneous energy harvesting and sensing systems," Ph.D. dissertation, University of New South Wales, Australia, 2025.

[7] M. W. Shafer and E. Garcia, "The power and efficiency limits of piezoelectric energy harvesting," *Journal of Vibration and Acoustics*, vol. 136, no. 2, p. 021007, 2014. https://doi.org/10.1115/1.4025996.

[8] T. Bailey and J. E. Hubbard Jr, "Distributed piezoelectric-polymer active vibration control of a cantilever beam," *Journal of Guidance, Control, and Dynamics*, vol. 8, no. 5, pp. 605-611, 1985. https://doi.org/10.2514/3.20029.

[9] T. L. Vo, L. N. P. Nguyen, N. N. Dang, S. H. Nguyen, "Response analysis and control of composite thin plate with piezoelectric actuators by finite element method," *Journal of Theoretical and Applied Mechanics*, vol. 63, no. 1, pp. 177-195, 2025. https://doi.org/10.15632/jtam-pl/194881.

[10] D. Maurya, P. Kumar, S. Khaleghian, R. Sriramdas, M. G. Kang, R. A. Kishore, et al., "Energy harvesting and strain sensing in smart tire for next generation autonomous vehicles," *Applied Energy*, vol. 232, pp. 312-322, 2018. https://doi.org/10.1016/j.apenergy.2018.09.183.

[11] M. Ikbal, M. Rizal, N. Ali, and T. E. Putra, "Design and experimental study of piezoelectric energy harvester integrated in rotating vehicle tire using end-cap system," *Results in Engineering*, vol. 25, p. 104195, 2025. https://doi.org/10.1016/j.rineng.2025.104195.

[12] J. Tang and K.-W. Wang, "Active-passive hybrid piezoelectric networks for vibration control: Comparisons and improvement," *Smart Materials and Structures*, vol. 10, no. 4, p. 794, 2001. https://doi.org/10.1088/0964-1726/10/4/325.

[13] F. Vidoli and Dell'Isola F, "Continuously distributed control of plates by electric networks with PZT actuators", in *Continuum Mechanics and Applications in Geophysics and the Environment*. Berlin, Heidelberg: Springer Berlin Heidelberg, 2001, pp. 92-110. https://doi.org/10.1007/978-3-662-04439-1_6.

[14] R. Zhang, L. Hyman, J. Ding, P. S. Keogh, and N. Y. Bailey, "Vibration suppression using piezoelectric actuator-based active flexure joints for high precision operations," *Mechanical Systems and Signal Processing*, vol. 235, p. 112816, 2025. https://doi.org/10.1016/j.ymssp.2025.112816.

[15] K. Uchino, "International Center for Actuators and Transducers," International Center for Actuators and Transducers, Penn State University, Rep. 40. 2003.

[16] A. Aabid, M. Hrairi, S. J. Mohamed Ali, and Y. E. Ibrahim, "Review of piezoelectric actuator applications in damaged structures: Challenges and opportunities," *ACS Omega*, vol. 8, no. 3, pp. 2844-2860, 2023. https://doi.org/10.1021/acsomega.2c06573.

[17] Y. Kitagawa, H. Tamai, and M. Takeshita, "Characteristics of piezoelectric dampers and their application to tall buildings as a smart structural system," In Proc. 13th World Conference on Earthquake Engineering, Vancouver, BC, Canada, Aug. 1-6, 2004.

[18] S. Roundy, "On the effectiveness of vibration-based energy harvesting," *Journal of Intelligent Material Systems and Structures*, vol. 16, no. 10, pp. 809-823, 2005. https://doi.org/10.1177/1045389X05054042.

[19] S. R. Moheimani and A. J. Fleming, "Fundamentals of piezoelectricity," in *Piezoelectric Transducers for Vibration Control and Damping*, London, UK: Springer, 2006, pp. 9-35.

[20] K. Al-Souqi, K. Kadri, and S. Emam, "A review on vibration control using piezoelectric shunt circuits," *Applied Sciences*, vol. 15, no. 11, p. 6035, 2025. https://doi.org/10.3390/app15116035.

[21] J. W. Sohn, S.-B. Choi, and C.-H. Lee, "Active vibration control of smart hull structure using piezoelectric composite actuators," *Smart Materials and Structures*, vol. 18, no. 7, p. 074004, 2009. https://doi.org/10.1088/0964-1726/18/7/074004.

[22] A. Khalatkar and V. Gupta, "Piezoelectric energy harvester for low engine vibrations," *Journal of Renewable and Sustainable Energy*, vol. 9, no. 2, 2017. https://doi.org/10.1063/1.4979501.

[23] P. Yingyong, P. Thainiramit, S. Jayasvasti, N. Thanach-Issarasak, and D. Isarakorn, "Evaluation of harvesting energy from pedestrians using piezoelectric floor tile energy harvester," *Sensors and Actuators A: Physical*, vol. 331, p. 113035, 2021. https://doi.org/10.1016/j.sna.2021.113035.

[24] J. Wang, X. Qin, Z. Liu, G. Ding, and G. Cai, "Experimental study on fatigue degradation of piezoelectric energy harvesters under equivalent traffic load conditions," *International Journal of Fatigue*, vol. 150, p. 106320, 2021. https://doi.org/10.1016/j.ijfatigue.2021.106320.

[25] H. Yang, L. Wang, Y. Hou, M. Guo, Z. Ye, X. Tong, et al., "Development in stacked-array-type piezoelectric energy harvester in asphalt pavement," *Journal of Materials in Civil Engineering*, vol. 29, no. 11, p. 04017224, 2017. https://doi.org/10.1061/(ASCE)MT.1943-5533.0002079.

[26] Y. Cao, A. Sha, Z. Liu, B. Luan, J. Li, and W. Jiang, "Electric energy output model of a piezoelectric transducer for pavement application under vehicle load excitation," *Energy*, vol. 211, p. 118595, 2020. https://doi.org/10.1016/j.energy.2020.118595.

[27] D. H. Jeon, J. Y. Cho, J. P. Jhun, J. H. Ahn, S. Jeong, S. Y. Jeong, et al., "A lever-type piezoelectric energy harvester with deformation-guiding mechanism for electric vehicle charging station on smart road," *Energy*, vol. 218, p. 119540, 2021. https://doi.org/10.1016/j.energy.2020.119540.

[28] C. Wang, S. Wang, Z. Gao, and Z. Song, "Effect evaluation of road piezoelectric micro-energy collection-storage system based on laboratory and on-site tests," *Applied Energy*, vol. 287, p. 116581, 2021. https://doi.org/10.1016/j.apenergy.2021.116581.

[29] Z. Liu, Y. Cao, A. Sha, H. Wang, L. Guo, and Y. Hao, "Energy harvesting array materials with thin piezoelectric plates for traffic data monitoring," *Construction and Building Materials*, vol. 302, p. 124147, 2021. https://doi.org/10.1016/j.conbuildmat.2021.124147.

[30] H. Kim, Y. Tadesse, and S. Priya, "Piezoelectric energy harvesting," in *Energy Harvesting Technologies*, S. Priya and D. J. Inman, Eds., Boston, MA, USA: Springer, 2009, pp. 3-39.

[31] S. S. Dani, A. Tripathy, N. R. Alluri, S. Balasubramaniam, and A. Ramadoss, "A critical review: The impact of electrical poling on the longitudinal piezoelectric strain coefficient," *Materials Advances*, vol. 3, no. 24, pp. 8886-8921, 2022. https://doi.org/10.1039/D2MA00559J.

[32] D. Ren, Y. Yin, C. Li, R. Chen, and J. Shi, "Recent advances in flexible ultrasonic transducers: From materials optimization to imaging applications," *Micromachines*, vol. 14, no. 1, p. 126, 2023. https://doi.org/10.3390/mi14010126.

[33] "Spring design equations," Engineers Edge, [online]. Available: https://www.springhouston.com/spring-information/spring-engineering.html. [Accessed Feb. 6, 2026].

[34] M. J. Giuliodori, H. L. Lujan, W. S. Briggs, G. Palani, and S. E. DiCarlo, "Hooke's law: Applications of a recurring principle," *Advances in Physiology Education*, vol. 33, no. 4, pp. 293-296, 2009. https://doi.org/10.1152/advan.00045.2009.

[35] P. Li, R. Yu, B. Zhang, Y. Wang, J. Chu, and K. Xue, "Study on Mechanical Behavior and Forming Simulation of Ultra-Thin 8011 Aluminum Alloy," *Journal of Materials Engineering and Performance*, vol. 34, no. 18, pp. 20636-20647, 2025. https://doi.org/10.1007/s11665-025-10725-5.

[36] ASM International, "Properties and selection: Nonferrous alloys and special-purpose materials," in ASM Handbook, vol. 2, Materials Park, OH, USA: ASM International, 1993. https://doi.org/10.31399/asm.hb.v02.9781627081627.

[37] B. Naveen Kumar, T. Babu, B. Tiwari, and R. N. P. Choudhary , "Review on PZT as a mechanical engineering material," *Ferroelectrics*, vol. 618, no. 1, pp. 125-138. https://doi.org/10.1080/00150193.2023.2271321.